Isothermal folding of G-quadruplexes

Published in final edited form as:
Methods. 2012 May ; 57(1): 47–55. doi:10.1016/j.ymeth.2012.04.006.

Isothermal Folding of G-quadruplexes

Robert D. Gray[a] and **Jonathan B. Chaires**[a]
[a]James Graham Brown Cancer Center, University of Louisville, 505 S. Hancock St., Louisville, KY 40202 USA

Abstract

Thermodynamic studies of G-quadruplex stability are an essential complement to structures obtained by NMR or x-ray crystallography. An understanding of the energetics of quadruplex folding provides a necessary foundation for the physical interpretation of quadruplex formation and reactivity. While thermal denaturation methods are most commonly used to evaluate quadruplex stability, it is also possible to study folding using isothermal titration methods. G-quadruplex folding is tightly coupled to specific cation binding. We describe here protocols for monitoring the cation-driven quadruplex folding transition using circular dichroism or absorbance, and for determination of the distribution of free and bound cation using a fluorescence indicator. Together these approaches provide insight into quadruplex folding at constant temperature, and characterize the linkage between cation binding and folding.

1. Introduction

G-quadruplexes are of great current interest because of their possible functional significance in both telomere maintenance and in the control of gene expression and additionally for their potential as novel drug targets [1–7]. Sequences that might fold into quadruplex structures are highly conserved and are non-randomly distributed within eukaryotic genomes [8–12]. The structural diversity G-quadruplexes has been elucidated by x-ray crystallographic and NMR studies [6, 7, 13–17], with a large number of structures on deposit in the Nucleic Acid Database. Structural studies alone, however, cannot provide a full understanding of quadruplex stability and reactivity. Energetic and kinetic studies are essential to attain an appropriate physical interpretation of quadruplex folding, stability and binding reactions.

Studies of quadruplex stability have most commonly used thermal denaturation methods in which changes in a spectroscopic signal (circular dichroism, UV absorbance, FRET fluorescence) are monitored as a function of temperature to measure unfolding transition curves [18–22]. The temperature at the transition midpoint (T_m) provides a quantitative measure of stability, and transition curves may be further analyzed (with assumptions about the reaction mechanism) to yield enthalpy values for quadruplex unfolding. Less commonly, calorimetric approaches (DSC, ITC) have been used to measure quadruplex denaturation or folding directly [23–25]. The energetics of G-quadruplex folding/unfolding was discussed in recent reviews [2, 26, 27].

Somewhat surprisingly, isothermal studies of quadruplex folding and unfolding are rare. This stands in contrast to protein and RNA folding where isothermal titration studies are

commonly used to explore the thermodynamics denaturation/renaturation reactions. Folding of G-rich oligonucleotides into quadruplex structures requires the participation of monovalent cations. Oligonucleotides containing runs of contiguous guanine residues tend to fold into four-stranded structures (quadruplexes) that consist of stacked rings of four Hoogsteen hydrogen-bonded G residues whose O6 atoms project into a cavity located in the center of the quartet. These O atoms can coordinate un-hydrated monovalent cations of appropriate size, including Na^+, K^+ and NH_4^+. X-ray crystallography shows that Na^+ binds the center of each quartet while K^+, owing to its larger size, shares O atoms contributed by two quartets in a tetragonal bipyrimidal arrangement [28, 29]. Thus the human telomeric model sequence d[A(GGGTTA)$_3$GGG] (Tel22), which contains three stacked G-quartets, binds three Na^+ or two K^+ within the central core of the quadruplex. It is also likely that Tel22 specifically binds (with lower affinity) additional K^+ to one or more external sites [30, 31]. These specific cation binding sites are distinct from cations associated by non-specific by electrostatic attraction to the highly negative phosphate backbone of the oligonucleotide. The latter cations are hydrated and are bound “territorially” in a highly mobile layer rather than be bound to any specific binding pocket.

Little information is available that allows thermodynamic analysis of the contribution of monovalent cation binding to the folding energetics of G-quadruplexes. This situation is in marked contrast to Mg^{2+}-driven folding of RNA structures in which several groups have dissected the energetic contributions of Mg^{2+} binding to folding. Our recent study of K^+-induced folding of Tel22 applied the approach of Draper et al. [32–35] to deduce that quadruplex folding is almost entirely driven by the energy of K^+ binding with little or no contribution from other weak interactions. This study utilized coordinated analysis of titration isotherms derived from circular dichroism (to monitor quadruplex folding) and a fluorescent potassium indicator (to monitor K^+ binding). The purpose of the present article is to give a detailed account of the approach we used to collect and analyze these cation binding isotherms.

2. Materials and Methods

2.1 Materials

The oligodeoxynucleotide Tel22 (d[A(GGGTTA)$_3$GGG]) was obtained in desalted, lyophilized form from Integrated DNA Technologies, Coralville, IA. It was dissolved at a concentration of 0.5 to 1 mM in 10 mM tetrabutylammonium phosphate, 1 mM EDTA, pH 7.0 (hereafter referred to as folding buffer). Oligonucleotide preparations used in the fluorescent K^+-indicator titrations were dialyzed against two changes of 0.5 liter each of folding buffer using a Float-A-Lyzer® G2 dialysis unit with a molecular weight cutoff of 100 – 500 and a volume of 1 ml (Spectrum laboratories, Inc., Rancho Dominquez, CA). The dialysis step partially removed a fluorescent impurity that interfered with the fluorescent K^+ indicator titrations. DNA concentrations were estimated from the 260 nm absorbance of suitable dilutions using an absorptivity coefficient of 228.5 mM^{-1} cm^{-1} supplied by the manufacturer. The K^+ indicator, the tetraammonium salt of PBFI, was purchased from Invitrogen, Carlsbad, CA. A 100 μM stock solution was prepared in deionized water and stored at −20 °C. The PBFI stock concentration was estimated from its absorbance at 345 nm using $\varepsilon = 42$ mM^{-1} cm^{-1}. A concentrated stock solution (3 M) of KCl was prepared in folding buffer; working dilutions of 10 mM, 100 mM and 1 M were prepared by diluting the stock solutions into folding buffer. All reagents other than those described above were from Sigma, St. Louis, MO.

2.2 Methods

2.2.1 Experimental protocol for assessing cation-driven G-quadruplex folding by CD and UV absorbance—The UV absorption and CD spectra of quadruplex DNA are significantly different from those of the corresponding unfolded oligonucleotide. The detailed features of the spectra depend on the topology of the fold (e.g. G-stack geometry and loop conformation) which in turn depends on the identity and concentration of the cation. Thus the extent of G-quadruplex folding as a function of cation concentration can be assessed by monitoring changes in CD or UV absorbance as aliquots of cation are added from a concentrated stock solution. The purpose of the folding buffer is to provide a buffered solution with a cation (tetrabutylammonium) that is too bulky to fit into the specific cation binding site within the quadruplex core, but which can interact territorially in accord with theory [36, 37] to neutralize the DNA polyelectrolyte to the necessary extent. Addition of cations (K^+ or Na^+) that bind specifically to the quadruplex coordination site then drives the quadruplex folding reaction.

2.2.1.1 Instrumental parameters for absorption and CD titrations: CD and UV absorption spectra were obtained with a Jasco J815 CD spectropolarimeter equipped with a Peltier cuvette thermostat and a magnetic stirrer for mixing the contents of a 1-cm path length silica cuvette (Jasco, Inc., Easton, MD). This instrument is capable of simultaneously recording both CD and absorbance spectra in digital format. Each spectrum, including a buffer blank, was scanned from 340 nm to 220 nm with instrumental settings of 1 nm/point, 1 nm spectral bandwidth, 200 nm/min scan speed, and digital integration time of 2 s. The average of four successive scans was stored as an Excel *.csv file consisting of 2-dimensional tables of wavelength vs. CD signal and absorbance at a particular cation concentration. A general discussion of CD methods as applied to nucleic acids is available [38].

2.2.1.2 Spectroscopic titration protocol: The following general protocol for assessing the dependence of quadruplex folding on cation concentration is appropriate for any spectroscopic method used to assess the state of folding in solution such as CD, absorbance or fluorescence.

1. Conduct a series of preliminary experiments to establish the approximate cation concentration required for 10%, 50% and 100% folding. Carry out multiple wavelength scans over time to establish that the spectra are stable. For KCl, the time required for formation of the initial folded state of Tel22 is relatively fast (<1–2 min) [39]; however full equilibration to the final mixture of states as assessed by CD may take up to 2 h (unpublished data).
2. Collect the CD and/or absorption spectra over the desired wavelength range (e.g. 340 nm to 220 nm) at constant temperature for ~20 cation concentrations spanning the range from 0 to ~100% of saturation. For accuracy in establishing the characteristics of the titration curve, most of the points should encompass the region 10–90% of saturation with sufficient points between 0–5% and 95–100% to establish pre- and post-transition baselines.
3. Subtract a blank (buffer alone) spectrum from each experimental spectrum and correct the spectra for dilution. This may be accomplished either by multiplying each data point by the appropriate dilution factor or by normalizing for oligonucleotide concentration after each addition of salt solution. For the absorption spectra, subtract the spectrum of the unfolded (zero added cation) from each of the cation-containing spectra to produce a set of difference spectra $\Delta A = A_{folded} - A_{unfolded}$. These difference spectra serve to amplify the somewhat subtle absorbance changes that accompany quadruplex folding.

2.3 Assessment of K^+ binding to G-quadruplexes using a fluorescent K^+ indicator

K^+ binding to quadruplex DNA can be assessed directly using a spectroscopic potassium indicator to assess [K^+] directly. PBFI, a fluorescent benzofuran isophthalate, undergoes a large increase in fluorescence intensity when K^+ binds [40]. This method, which we modeled after the cation indicator procedure of Grilley et al. [41] for rigorously analyzing the linkage between Mg^{2+} binding and RNA folding, allows estimation of bound cation as a function of free cation activity by comparing the cation:indicator binding isotherms in the presence and absence of polynucleotide.

2.3.1 Simulation of Fluorescent Indicator K^+-Titrations—To define concentrations that allow accurate measurement of K^+ binding to quadruplex DNA, we first carried out a set of K^+-binding simulations comparing the binding isotherms for K^+-indicator in the presence and absence of an oligonucleotide that binds K^+. The set of equilibria shown in Scheme 1 were used to describe competitive binding of K^+ to PBFI and DNA assuming cooperative binding of 2 K^+/DNA and using reasonable values for the respective K^+ dissociation constants of the various species.

The dissociation constant for PBFI is taken from the literature while those for DNA give a reasonable approximation for the cooperative K^+ binding to 143D. The simulation was carried out with the program SpectFit/32 (Spectrum Software Associates, Marlborough, MA); the results are shown in Fig. 1.

The simulation reveals that achieving a measurable difference between the control titrations and the DNA-containing titrations requires comparatively high concentrations of oligonucleotide (e.g. 300 – 500 μM) at 1 μM indicator.

2.3.1.1 Instrumental parameters for PBFI titrations with KCl: Fluorescence spectra for oligodeoxynucleotide/PBFI-KCl titrations were obtained with a FluoroMax-3® instrument (Horiba Instruments, Inc., Edison, NJ). Titrations were carried out by adding small volumes of concentrated KCl solutions to 150 μL of dilute indicator containing the oligonucleotide of interest in a silica micro-cuvette of path length 3 mm × 3 mm (Starna Cells, Inc., Atascadero, CA). After thorough mixing, the emission spectrum of the PBFI was scanned from 400–600 nm (5 nm bandwidth). The excitation wavelength was 350 nm (2 nm bandwidth) and the cuvette was maintained at 25 °C by circulating water through the cell holder from a refrigerated water bath (Jubalo, Inc., Allentown, PA). PBFI emission spectra were corrected by subtracting a buffer or oligonucleotide/buffer emission spectrum as appropriate. Emission spectra for buffer/PBFI titrations were corrected for dilution by the added KCl (maximum of ~20%). Control titrations of the oligonucleotide solutions with KCl showed that a compensating small increase in apparent emission intensity at 472 nm with increasing [KCl] made correction for dilution unnecessary. Titration curves were constructed by plotting fluorescence intensity measured at 472 nm (the maximum in the difference between K^+-bound and K^+-free PBFI) vs. [KCl].

2.3.1.2 Protocol for K^+-indicator titrations

1. Place 150 μL of buffer or oligonucleotide of known concentration (400–500 μM) in a micro fluorescence cuvette. Set excitation wavelength to 350 nm. Adjust excitation and emission bandwidths to 2 nm and 5 nm. Equilibrate sample at desired temperature. Scan emission spectrum (blank) from 400 to 600 nm.
2. Prepare a 100 μM stock solution of PBFI. Add sufficient PBFI from the concentrated stock to give a final concentration of 1 μM. Scan the emission spectrum as above.

3. Add small (1–5 μL) aliquots of KCl from concentrated stock solutions to cover a range of K^+ concentrations from approximately 20 μM to 100 mM. Mix thoroughly and scan emission spectrum as in step 1 above. KCl concentrations should be chosen to ensure that the points in the titration curve between 10% and 90% of saturation are well represented and with sufficient points to establish the lower and upper ends of the titration curve.

4. Correct the data set for dilution and plot the resulting fluorescence intensity at 472 nm vs. added [KCl].

3. Theory/calculations

3.1 Single wavelength analysis of folding isotherms

For preliminary data analysis, the cation titration data obtained by monitoring the binding process at a single wavelength are fit to a modified form of the Hill equation (Eq. 1) to estimate the four parameters that describe the titration: values for the experimental variable at the extremes of the titration curve (S_0 and S_{100}), the midpoint cation concentration ($K_{0.5}$), and the Hill coefficient n:

$$S_i=(S_0-S_{100})[M^+]^n/(K_{0.5}{}^n+[M^+]^n)+S_0 \quad (1)$$

where S_i is the value of the signal (absorbance, CD or fluorescence intensity) after the i^{th} addition of cation. S_0, S_{100}, $K_{0.5}$, and n were optimized by a non-linear least squares procedure using the program Origin 7.0 (OriginLab Corp., Northhampton, MA). $K_{0.5}$ and n provide quantitative characterization of the isothermal folding process. $K_{0.5}$ is the cation concentration at the transition midpoint, and might be thought of as analogous to a T_m value obtained from thermal denaturation studies. The Hill coefficient n is a measure of the cooperativity of the folding transition. While $K_{0.5}$, and n are useful quantitative measures of the folding transition, we caution that they are phenomenological parameters that do not refer to any physically meaningful reaction mechanism from which thermodynamic information might be derived [42].

It is often desirable to compare titration curves obtained at different wavelengths or measured by different methods to check for the possibility of intermediates in the titration or internal consistency of the data sets. To facilitate direct comparison of different datasets, it is useful to convert the data into saturation curves. The fractional signal change Y_i at each $[M^+]_i$ is calculated from

$$Y_i=(S_i-S_0)/(S_{100}-S_0) \quad (2)$$

where S_i is the signal intensity at the ith M^+ addition, S_0 and S_{100} are the signal intensities at 0 and 100% of saturation determined as described in Eq. 1.

3.2 SVD analysis of folding isotherms

A rigorous method of data analysis that facilitates analysis of complex data sets such as multi-wavelength titration data is the method of singular value decomposition (SVD). Modern spectroscopic instruments generally provide digitized data sets consisting of a two-dimensional table (vector) of wavelengths vs. the spectroscopic signal intensity (e.g. fluorescence, absorbance, or CD). Thus it is easy to collect an entire spectral response over a wavelength range of interest as a function of an experimental variable. Since the different quadruplex topologies generally exhibit distinct spectral properties, it is possible to detect the evolution of structures as a function of the experimental variable by measuring complete spectra.

The mathematical formalism of SVD provides convenient method of globally analyzing complex data sets to aid in determining the number of statistically significant species contributing to a set of signal intensities that vary with changes in an experimental variable. SVD also provides a rigorous means of smoothing data sets without distorting the response curves. We previously described application of SVD to the analysis of thermal melting curves for nucleic acids [43], NaCl-induced changes in DNA secondary structures [44, 45], and K^+-induced folding of Tel22 [30, 31]. An overview of SVD analysis as applied to the cation-induced folding of Tel22 is provided below. The reader is directed to a number of more complete reviews for further details [44, 46–48].

Individual 2-dimensional data sets consisting of optical spectra measured as a function of $[M^+]$ are assembled into a 3-dimensional matrix $\boldsymbol{D}$ consisting of j columns of spectral response as a function of wavelength λ_j at constant $[M^+]$ and i rows containing the spectral response as a function of $[M^+]_j$ at constant λ. Thus, any element of the matrix $\boldsymbol{D_{i,j}}$ will correspond to the spectroscopic signal at λ_j at $[M^+]_i$. A plot of column vectors j for different rows i will yield a family of plots showing the dependency of the signal strength on λ_j at each $[M^+]_i$. Correspondingly, plots of the row vectors i will depict a family of binding isotherms for each λ_j

The SVD method decomposes the data matrix $\boldsymbol{D}$ into $\boldsymbol{U}$, $\boldsymbol{S}$ and $\boldsymbol{V}$ matrices such that $\boldsymbol{D} = \boldsymbol{USV^T}$. The $\boldsymbol{U}$ matrix contains the "basis spectra" which are normalized spectral shapes that may be combined to form the spectra of the data matrix provided the data set can be fit to an explicit mechanism (such as a binding equilibrium). (It is worth emphasizing that the basis spectra are *not* the absolute spectra of the species. The absolute spectra of the significant species can be only be calculated by fitting the data set to a specific mechanism or by using the technique of evolving factor analysis [49].) The $\boldsymbol{S}$ matrix is a diagonal matrix that contains the weights of the spectral components (the singular values). The $\boldsymbol{V}$ matrix contains the amplitudes of the signal intensity as a function of the experimental variable (e.g. $[M^+]$). Thus the $\boldsymbol{U}$ matrix elements resemble the spectra of the individual species, the $\boldsymbol{V}$ matrix elements resemble a titration curve for each of the components, revealing their rise and decay as the titration proceeds, and the $\boldsymbol{S}$ matrix indicates the relative contribution of each component to the data set.

A challenging aspect of SVD is deciding which components are "significant." One method is to determine the relative magnitudes of the $\boldsymbol{S}$ elements in relation to the noise level. This can be assessed from a "scree" plot of the relative variance RV vs. the rank i of S_i [50]. The RV of each singular value is calculated from $RV=S_i^2/\sum S_i^2$ where S_i is the singular value and the summation is carried out over all singular values. By definition, there will be a singular value corresponding to each row (λ) of the data matrix. Additional parameters that may be useful in determining the number of significant species are the autocorrelation coefficients $C(X_i) = \Sigma X_{j,i} \cdot X_{j+1,i}$ of the $\boldsymbol{U}$ and $\boldsymbol{V}$ elements. These coefficients can range from +1 to −1 where values approaching+1 are highly correlated while values approaching 0 indicate no correlation. Defining an exact cutoff in the autocorrelation coefficient for "significance" can be ambiguous, although a value of +0.8 may be taken to indicate significant variation of signal with the independent variable. For this reason, we tend to rely most on the scree plot to assess the significance of a particular spectroscopic species to the overall signal.

As mentioned above, an additional benefit of SVD analysis is that a "smoothed" data set can be reconstructed by re-combining only those elements of $\boldsymbol{D}$ which are statistically significant. Thus SVD automatically filters the data to remove noise. Subtraction of this reduced data matrix from the experimental data matrix yields a matrix of residuals that

exhibits no discernible pattern if significant data have been removed. This process also can aid in deciding which species are significant.

We use the mathematical package *MatLab* 7.1 (MathWorks, Natick, MA) to perform SVD analyses on a personal computer. Other analysis suites such as *Mathmatica* (Wolfram Research, Inc., Champaign, IL) contain built-in modules for SVD analysis as well.

4. Analysis of titration curves

4.1 Stepwise analysis of single wavelength data sets

1. Plot the family of titration curves to ascertain where the maximum changes in signal occur in the spectral region scanned.
2. Choose at least two titrations at wavelengths of maximal change. Fit each data set to the modified Hill equation. This provides a convenient indicator of the cation concentration for half-maximal folding as well as the degree of cooperativity in binding reaction.
3. Using the fitted values of S_0 and S_{100} as starting and endpoints for the titration, convert individual data sets into saturation plots Y vs. $[M^+]$ as described by Eq. 2 to allow comparison of the data sets.

4.2 Stepwise analysis of multiple wavelength data sets by SVD

1. Assemble the spectral record for each $[M^+]$ into a data matrix $\boldsymbol{D}$. In the example shown in Fig. 2 below, the data set consists of 121 wavelengths and 24 KCl concentrations between 0 and 100 mM, so $\boldsymbol{D}$ will have 24 columns and 121 rows to produce a 121×24 matrix.
2. Subject $\boldsymbol{D}$ to SVD analysis using a program such as *MatLab*. As stated above, SVD factors $\boldsymbol{D}$ into $\boldsymbol{U}$, $\boldsymbol{S}$ and $\boldsymbol{V}$ matrices which for the example here, consist respectively of a 121×24 matrix, a 24×24 diagonal matrix, and a 24×24 matrix. The matrix $\boldsymbol{US} = \boldsymbol{U}\times\boldsymbol{S}$ contains the basis spectra weighted by their contribution to the total signal change.
3. Calculate the autocorrelation coefficients for the $\boldsymbol{U}$ and $\boldsymbol{V}$ matrices and the fractional variance for each singular values (24 in this example).
4. Plot the $\boldsymbol{U}\times\boldsymbol{S}$ vectors (weighted basis spectra) vs. λ and the $\boldsymbol{V}$ vectors vs. [KCl]. Examine the basis spectra for distinguishable spectral shapes and the $\boldsymbol{V}$ plot for trends that resemble a titration curve.
5. Plot the singular values, relative variances and autocorrelation coefficients to compare their relative magnitudes and signs (for the autocorrelation coefficients) as an aid in deciding on the significance of each component to the total data set (i.e. which components exceed the noise in the data set).

4. Results

4.1 CD and absorbance titrations

Fig. 2 shows an example of a titration of Tel22 by KCl in which the extent of folding is monitored simultaneously by CD (panel A) and differential absorption (panel B) spectroscopies. Both families of spectra clearly exhibit several wavelength maxima and minima (shown in the figures) which could be chosen for fitting the titration curves to Eq. 1. Figures 2C and 2D show the dependence of CD and absorbance signals on [KCl] at different wavelengths near the spectral maxima in each family (287 and 269 nm for the CD titrations and 296 and 263 nm for absorbance titrations). The lines in the figures 2C and 2D were

derived by fitting the data points from 0 to ~10 mM KCl to Eq. 1. The points in grey in the figures were omitted from the fitting procedure because they appear to represent a secondary process such as binding of additional cations at higher [KCl] [30, 31]. The least-squares optimized parameters are shown in the figures. The fitted $K_{0.5}$ and n values for the CD data are nearly identical; however the absorbance method gives somewhat different parameter values at the two wavelengths (particularly for n), suggesting that this method may sense different folding events, particularly at higher [KCl].

4.1.1 SVD analysis of CD and absorbance titrations—SVD analysis is used to define the number of spectroscopically distinct species required to describe the wavelength dependence of the titrations, and thus give an indication of the need to incorporate intermediate species in the folding mechanism. The results of an SVD analysis of the data sets in Fig. 2 are summarized in Figs. 3–5 and Table 1. Fig. 3 shows the three highest ranking basis spectra for the UV difference spectra and the CD titrations with KCl (individual species labeled 1, 2, and 3). As expected, the most significant basis spectrum 1 resembles the absolute (difference or CD) spectra of the folded species and spectrum 2 resembles the spectrum of the unfolded species. For both data sets, the basis spectrum of the third ranking species 3 is much smaller in magnitude compared to the two more significant species.

Fig. 4 shows the variation in in the amplitude of the $\boldsymbol{V}$ vectors with [KCl] corresponding to the three most significant species as taken from the $\boldsymbol{V}$ matrices for the CD and absorbance titrations. The amplitude of the vectors associated with components 1 and 2 clearly resembles the titration curves in Fig. 2C and 2D. Their variation with [KCl] is not random as shown by the autocorrelation coefficients of 0.9956 and 0.9021 for the CD. For the absorbance data, only the first $\boldsymbol{V}$ vector shows a strong autocorrelation coefficient of 0.951; the second is less strongly correlated with [KCl] (0.6195). The $\boldsymbol{V}$ vector for the less significant third species in both data sets apparently also varies systematically with [KCl], but the autocorrelation coefficients of 0.6743 and 0.6791 do not meet the +0.8 criterion for significance. The shape of the curves suggests the possibility of an intermediate, but the relative magnitude and spectral properties suggests that the population is quite small during the titration. This behavior is expected for a highly cooperative folding transition.

Analysis of the relative variance RV of each component supports the conclusion that the folding reaction is essentially two-state. Table 1 shows the singular values (relative weights) and RVs associated with the five highest ranking species along with their relative contribution to the total variance of the two data sets. In both sets the first two components have the largest values and contribute over 99.9% of the total signal variance. Thus we conclude that to a high degree of approximation, the folding equilibrium of Tel22 in KCl can be represented as two-state U ↔ F transition.

4.1.2 Estimation of free energy of folding from titration data—The two-state approximation allows calculation of an apparent equilibrium constant for the folding process from the equation $K_{app,i}=Y_i/(1-Y_i)$, [Note: Eq. 2 in ref [31]contains a typographical error] where Y_i is defined at $[KCl]_i$ by Eq. 2. The titration in Fig. 2C yields the linear relation

$$\ln K_{app}=(12.94 \pm 0.18)+(1.56 \pm 0.02)\ln[KCl]$$

with a correlation coefficient of 0.998. The standard deviations of the fitted parameters are indicated. The coefficient of the second term is related to the difference in the number of cations bound between the unfolded and folded states. The apparent Gibbs free energy

ΔG_{app} for folding at any [KCl] can then be estimated from the standard relationship $\Delta G_{app,i} = -RT\ln K_{app,i.}$

4.2 PBFI-K^+ fluorescence titrations

Titration of DNA in the presence of a cation indicator provides an alternative way of investigating the cation binding – folding equilibria. Fig. 5 illustrates the changes in fluorescence maximum and emission intensity elicited by binding K^+ to PBFI. The difference emission spectra $\Delta F = F_{complex} - F_{free}$ is shown in panel B. There is approximately an 18-fold increase in emission intensity at 472 nm when PBFI is converted to its complex with K^+.

Fig. 6A shows the analysis of the emission intensity at 472 nm for PBFI in buffer as a function of added [KCl] compared to the intensity in the presence of Tel22. The lines represent a least squares fit of the data to Eq. 1; the optimized fitting parameters are given in the figure. Fig. 6B shows the data normalized according to Eq. 2. This presentation clearly shows a shift to the right of the DNA-containing titration indicative of K^+ binding to DNA resulting from K^+ binding to the DNA and thus not available for binding to the indicator.

Figure 7 shows an expanded representation of the data in Figure 5B which illustrates schematically the partitioning of the added (total) K^+ into bound and free fractions. The K^+ binding stoichiometry ν can then be estimated using Eq. 3:

$$\nu=[K^+]_{bound}/[DNA]=([K^+]_{total}-[K^+]_{ref})/[DNA]. \quad (3)$$

4.3 Correlation of folding and K^+ binding

Figure 8 compares the K^+ binding stoichiometry for Tel22 calculated using Eq. 3 with the extent of folding as assessed by CD. Two interesting conclusions are apparent from these data. First, as depicted in Panel B, Tel22 binds more than the two K^+ expected if the only mode of cation binding is coordination between the three G-stacks of Tel22. Similar results were obtained for the hybrid-1-forming quadruplex 2GKU [31]. The nature of these binding sites is not entirely clear, but may represent specific sites resulting from certain folding geometries [30]. Interestingly, a recent high-resolution structure of a quadruplex formed by the c-kit promoter sequence revealed that potassium and magnesium ions have unexpected but significant structural roles in stabilizing particular quadruplex loops and grooves [51]. These cation interactions are distinct from and are in addition to potassium ions in the ion channel at the center of all quadruplex structures. The additional potassium ions that bind after completion of folding seen in Fig. 8B can plausible be assigned to similar types of sites. The second interesting feature is that quadruplex formation as assed by CD is essentially complete by 2–3 mm KCl, a K^+ concentration that corresponds to a binding stoichiometry of 2:1 (dashed lines in Figure 8).

5. Conclusions

Isothermal titration methods provide valuable new approaches for quantitative studies of quadruplex folding and cation binding. These methods complement structural studies and commonly used thermal denaturation methods used to determine quadruplex stability. Physical insight into the forces that drive quadruplex folding and subsequent reactivity need all such complementary approaches for a full understanding of the fundamental processes at work.

Acknowledgments

Supported by grant CA35635 from the National Cancer Institute.

References

1. Huppert JL. Four-stranded nucleic acids: structure, function and targeting of G-quadruplexes. Chem Soc Revs. 2008; 37:1375–1384. [PubMed: 18568163]
2. Lane AN, Chaires JB, Gray RD, Trent JO. Stability and kinetics of G-quadruplex structures. Nucleic Acids Res. 2008
3. Lipps HJ, Rhodes D. G-quadruplex structures: in vivo evidence and function. Trends Cell Biol. 2009; 19:414–422. [PubMed: 19589679]
4. Mergny JL, Helene C. G-quadruplex DNA: a target for drug design. Nat Med. 1998; 4:1366–1367. [PubMed: 9846570]
5. Neidle S. The structures of quadruplex nucleic acids and their drug complexes. Current Op Structural Biol. 2009; 19:239–250.
6. Collie GW, Parkinson GN. The application of DNA and RNA G-quadruplexes to therapeutic medicines. Chem Soc Revs. 2011; 40:5867–5892. [PubMed: 21789296]
7. Balasubramanian S, Hurley LH, Neidle S. Targeting G-quadruplexes in gene promoters: a novel anticancer strategy? Nat Rev Drug Discov. 2011; 10:261–275. [PubMed: 21455236]
8. Huppert JL, Balasubramanian S. Prevalence of quadruplexes in the human genome. Nucleic Acids Res. 2005; 33:2908–2916. [PubMed: 15914667]
9. Huppert JL, Balasubramanian S. G-quadruplexes in promoters throughout the human genome. Nucleic Acids Res. 2007; 35:406–413. [PubMed: 17169996]
10. Eddy J, Maizels N. Gene function correlates with potential for G4 DNA formation in the human genome. Nucleic Acids Res. 2006; 34:3887–3896. [PubMed: 16914419]
11. Eddy J, Maizels N. Conserved elements with potential to form polymorphic G-quadruplex structures in the first intron of human genes. Nucleic Acids Res. 2008; 36:1321–1333. [PubMed: 18187510]
12. Huppert JL. Hunting G-quadruplexes. Biochimie. 2008; 90:1140–1148. [PubMed: 18294969]
13. Patel DJ, Phan AT, Kuryavyi V. Human telomere, oncogenic promoter and 5′-UTR G-quadruplexes: diverse higher order DNA and RNA targets for cancer therapeutics. Nucleic Acids Res. 2007; 35:7429–7455. [PubMed: 17913750]
14. Phan AT. Human telomeric G-quadruplex: structures of DNA and RNA sequences. FEBS J. 2010; 277:1107–1117. [PubMed: 19951353]
15. Burge S, Parkinson GN, Hazel P, Todd AK, Neidle S. Quadruplex DNA: sequence, topology and structure. Nucleic Acids Res. 2006; 34:5402–5415. [PubMed: 17012276]
16. Yang D, Okamoto K. Structural insights into G-quadruplexes: towards new anticancer drugs. Future Med Chem. 2010; 2:619–646. [PubMed: 20563318]
17. Dai J, Carver M, Yang D. Polymorphism of human telomeric quadruplex structures. Biochimie. 2008; 90:1172–1183. [PubMed: 18373984]
18. De Cian A, Guittat L, Kaiser M, Sacca B, Amrane S, Bourdoncle A, Alberti P, Teulade-Fichou MP, Lacroix L, Mergny JL. Fluorescence-based melting assays for studying quadruplex ligands. Methods (San Diego, CA). 2007; 42:183–195.
19. Mergny, JL.; Lacroix, L. UV Melting of G-Quadruplexes. In: Beaucage, Serge L., et al., editors. Current protocols in nucleic acid chemistry. Vol. Chapter 17. 2009. p. 11
20. Mergny JL, Phan AT, Lacroix L. Following G-quartet formation by UV-spectroscopy. FEBS Lett. 1998; 435:74–78. [PubMed: 9755862]
21. Darby RA, Sollogoub M, McKeen C, Brown L, Risitano A, Brown N, Barton C, Brown T, Fox KR. High throughput measurement of duplex, triplex and quadruplex melting curves using molecular beacons and a LightCycler. Nucleic Acids Res. 2002; 30:e39. [PubMed: 11972354]
22. Rachwal PA, Fox KR. Quadruplex melting. Methods (San Diego, CA). 2007; 43:291–301.

23. Antonacci C, Chaires JB, Sheardy RD. Biophysical characterization of the human telomeric $(TTAGGG)_4$ repeat in a potassium solution. Biochemistry. 2007; 46:4654–4660. [PubMed: 17381076]
24. Majhi PR, Qi J, Tang CF, Shafer RH. Heat capacity changes associated with guanine quadruplex formation: an isothermal titration calorimetry study. Biopolymers. 2008; 89:302–309. [PubMed: 18183583]
25. Olsen CM, Gmeiner WH, Marky LA. Unfolding of G-quadruplexes: energetic, and ion and water contributions of G-quartet stacking. J Phys Chem B. 2006; 110:6962–6969. [PubMed: 16571009]
26. Chaires JB. Human telomeric G-quadruplex: thermodynamic and kinetic studies of telomeric quadruplex stability. FEBS J. 2010; 277:1098–1106. [PubMed: 19951355]
27. Lane AN. The stability of intramolecular DNA G-quadruplexes compared with other macromolecules. Biochimie. 2012; 94:277–286. [PubMed: 21854828]
28. Haider S, Parkinson GN, Neidle S. Crystal structure of the potassium form of an *Oxytricha nova* G-quadruplex. J Mol Biol. 2002; 320:189–200. [PubMed: 12079378]
29. Parkinson GN, Lee MP, Neidle S. Crystal structure of parallel quadruplexes from human telomeric DNA. Nature. 2002; 417:876–880. [PubMed: 12050675]
30. Gray RD, Petraccone L, Trent JO, Chaires JB. Characterization of a K^+-induced conformational switch in a human telomeric DNA oligonucleotide using 2-aminopurine fluorescence. Biochemistry. 2010; 49:179–194. [PubMed: 19961180]
31. Gray RD, Chaires JB. Linkage of cation binding and folding in human telomeric quadruplex DNA. Biophy Chem. 2011; 159:205–209.
32. Grilley D, Soto AM, Draper DE. Direct quantitation of Mg^{2+}-RNA interactions by use of a fluorescent dye. Methods Enzymol. 2009; 455:71–94. [PubMed: 19289203]
33. Leipply D, Lambert D, Draper DE. Ion-RNA interactions thermodynamic analysis of the effects of mono- and divalent ions on RNA conformational equilibria. Methods Enzymol. 2009; 469:433–463. [PubMed: 20946802]
34. Draper DE. RNA folding: thermodynamic and molecular descriptions of the roles of ions. Biophys J. 2008; 95:5489–5495. [PubMed: 18835912]
35. Draper DE. A guide to ions and RNA structure. RNA. 2004; 10:335–343. [PubMed: 14970378]
36. Manning GS. The molecular theory of polyelectrolyte solutions with applications to the electrostatic properties of polynucleotides. Q Rev Biophys. 1978; 11:179–246. [PubMed: 353876]
37. Record MT Jr, Anderson CF, Lohman TM. Thermodynamic analysis of ion effects on the binding and conformational equilibria of proteins and nucleic acids: the roles of ion association or release, screening, and ion effects on water activity. Q Rev Biophys. 1978; 11:103–178. [PubMed: 353875]
38. Bishop, GR.; Chaires, JB. Characterization of DNA structures by circular dichroism. In: Beaucage, Serge L., et al., editors. Current protocols in nucleic acid chemistry. Vol. Chapter 7. 2003. p. 11
39. Gray RD, Chaires JB. Kinetics and mechanism of K^+- and Na^+-induced folding of models of human telomeric DNA into G-quadruplex structures. Nucleic Acids Res. 2008; 36:4191–4203. [PubMed: 18567908]
40. Minta A, Tsien RY. Fluorescent indicators for cytosolic sodium. J Biol Chem. 1989; 264:19449–19457. [PubMed: 2808435]
41. Grilley D, Soto AM, Draper DE. Direct quantitation of Mg^{2+}-RNA interactions by use of a fluorescent dye. Methods Enzymol. 2009; 455:71–94. [PubMed: 19289203]
42. Holt JM, Ackers GK. The Hill coefficient: inadequate resolution of cooperativity in human hemoglobin. Methods Enzymol. 2009; 455:193–212. [PubMed: 19289207]
43. Gray, RD.; Chaires, JB. Analysis of multidimensional G-quadruplex melting curves. In: Beaucage, Serge L., et al., editors. Current protocols in nucleic acid chemistry. Vol. Chapter 17. 2011. p. 14
44. Haq I, Chowdhry BZ, Chaires JB. Singular value decomposition of 3-D DNA melting curves reveals complexity in the melting process. Eur Biophys J. 1997; 26:419–426. [PubMed: 9404005]
45. Sheardy RD, Suh D, Kurzinsky R, Doktycz MJ, Benight AS, Chaires JB. Sequence dependence of the free energy of B-Z junction formation in deoxyoligonucleotides. J Mol Biol. 1993; 231:475–488. [PubMed: 8510158]

46. DeSa RJ, Matheson IB. A practical approach to interpretation of singular value decomposition results. Methods Enzymol. 2004; 384:1–8. [PubMed: 15081677]

47. Hendler RW, Shrager RI. Deconvolutions based on singular value decomposition and the pseudoinverse: a guide for beginners. J Biochem Biophys Methods. 1994; 28:1–33. [PubMed: 8151067]

48. Henry R, Hofrichter J. Singular value decomposition: application to analysis of experimental data. Methods Enzymol. 1992; 210:129–191.

49. Keesey RL, Ryan MD. Use of evolutionary factor analysis in the spectroelectrochemistry of *Escherichia coli* sulfite reductase hemoprotein and a Mo/Fe/S cluster. Anal Chem. 1999; 71:1744–1752. [PubMed: 10330905]

50. Catell RB. The scree test for the number of factors. Genetic Psychology Monographs. 1963; 1:245–276.

51. Wei D, Parkinson GN, Reszka AP, Neidle S. Crystal structure of a c-kit promoter quadruplex reveals the structural role of metal ions and water molecules in maintaining loop conformation. Nucleic Acids Res. 2012 [Epub ahead of print]. 10.1093/nar/gks023

52. Gray RD, Petraccone L, Buscaglia R, Chaires JB. 2-aminopurine as a probe for quadruplex loop structures. Methods Mol Biol. 2010; 608:121–136. [PubMed: 20012419]

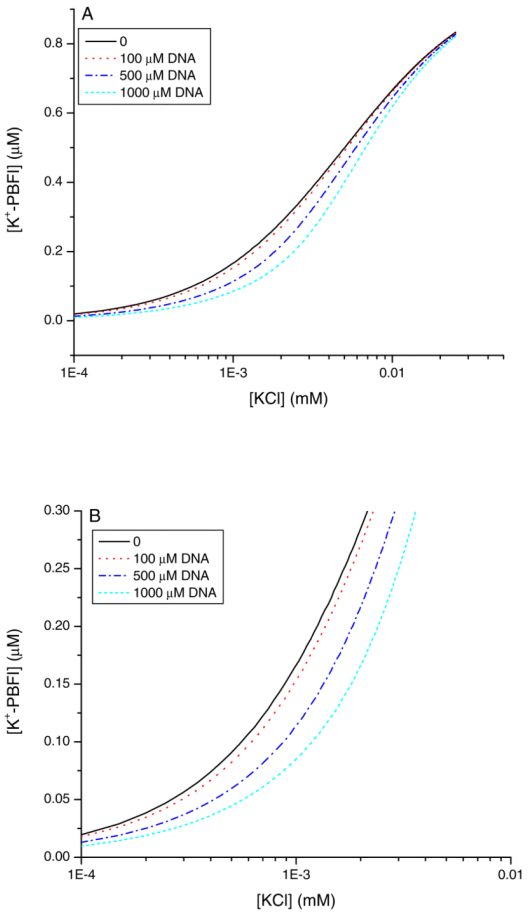

Fig. 1.

Simulation of binding of K^+ to the fluorescent indicator PBFI in the absence and presence of varying concentrations of quadruplex DNA. The simulation was carried out using the program SpectFit/32 using the three reactions shown in Scheme 1 and the dissociation constants and DNA concentrations indicated in the figure. [PBFI] was 1 μM. Panel B shows an expanded version of Panel A.

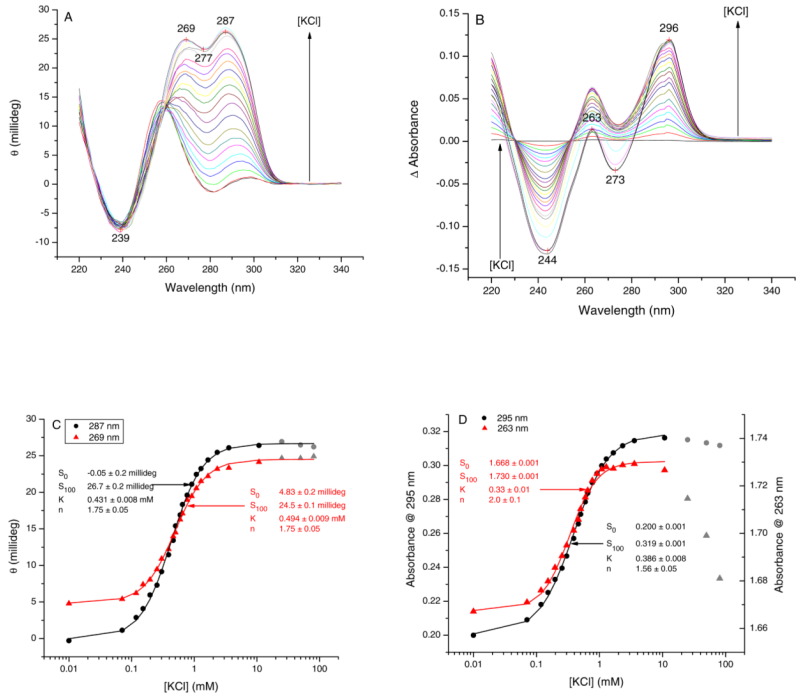

Fig. 2.

Titration of Tel22 with KCl measured by CD (panel A) and differential absorption (panel B) spectroscopies. The vertical arrows indicate increasing [KCl]. Panels C and D show the [KCl]-dependence of the spectroscopic signal determined at single wavelengths. The lines show the best fit of the points to Eq. 1 with the optimized parameters and their standard deviations given in the figure. The points in grey in panel D were not included in the least squares fitting analysis. The gradual decrease in the changes in absorbance at > 10 mM KCl (grey symbols) may reflect K^+-dependent conformational changes as previously observed at higher [KCl] [52]. Conditions: 7.7 μM Tel22, 10 mM tetrabutylammonium phosphate, 1 mM EDTA, pH 7.0, 20 °C. [KCl] varied from 0.01 to 81 mM.

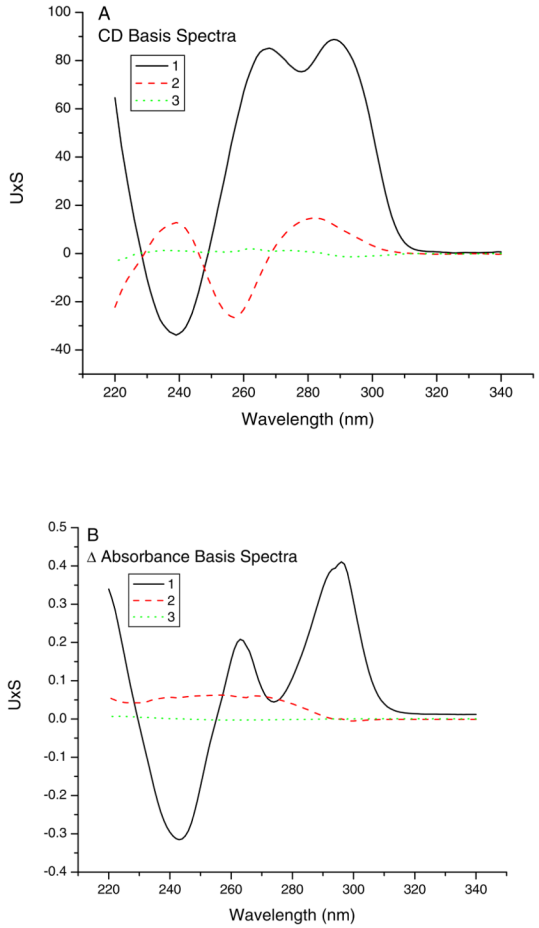

Fig. 3.
Basis spectra for the three most significant components as derived by SVD analysis of the data sets of Fig. 2.

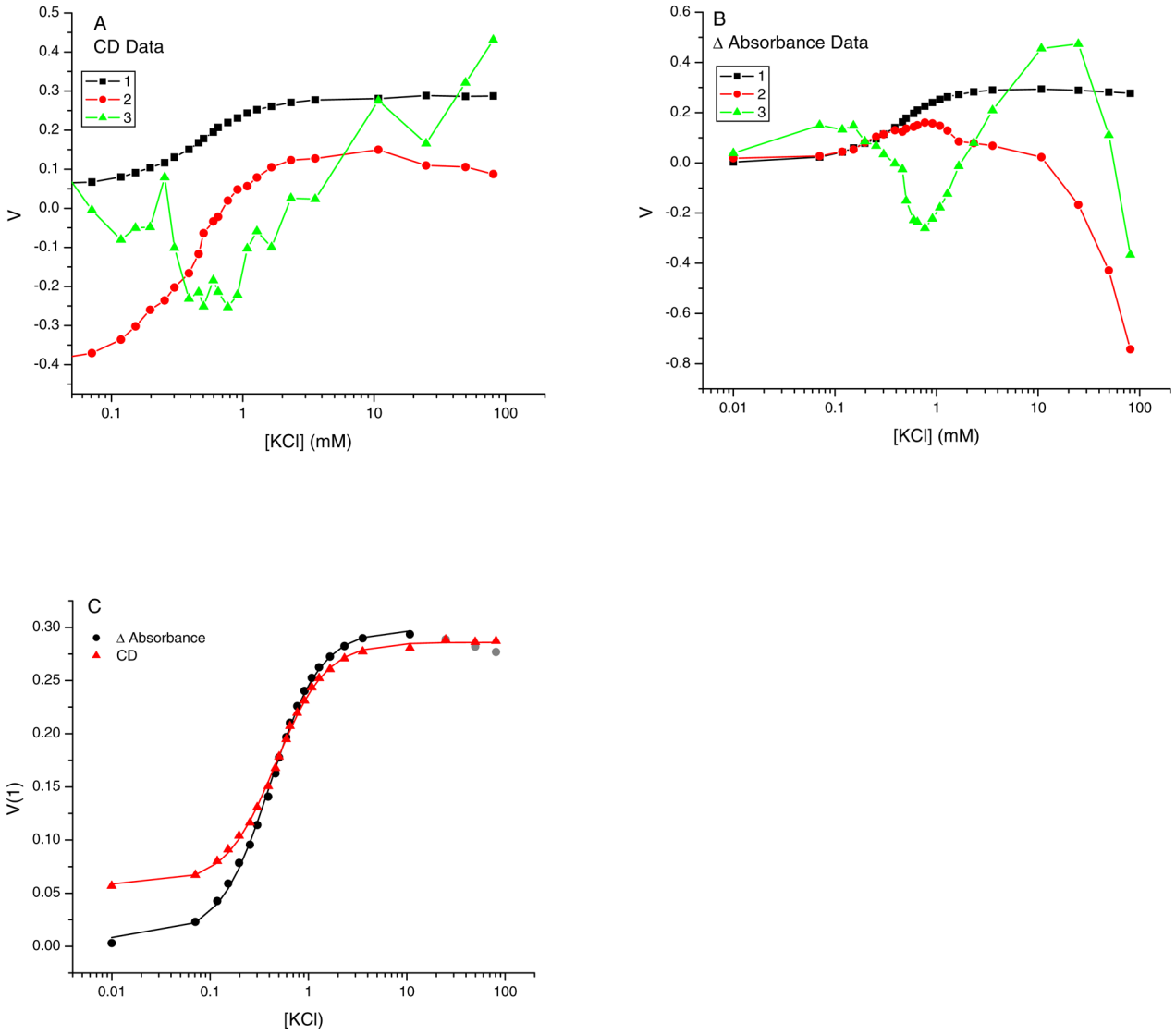

Fig. 4.
Amplitudes of the first three ***V*** vectors corresponding to the basis spectra in Fig. 3.

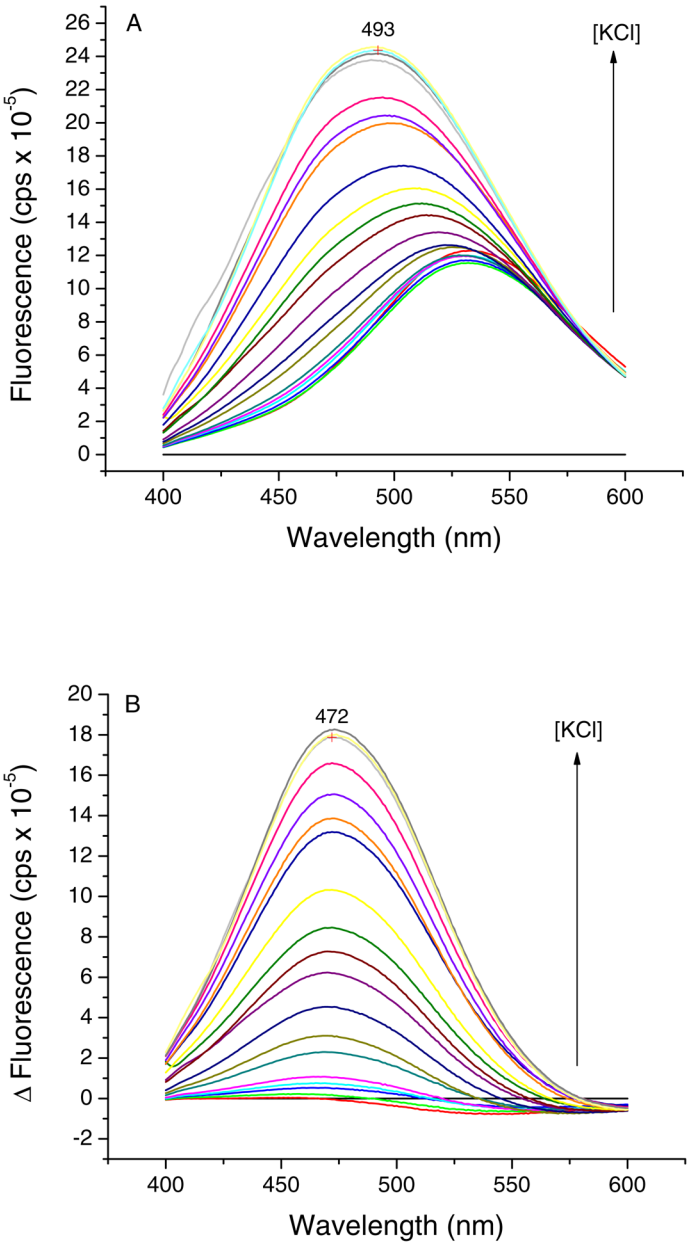

Fig. 5.

Effect of K^+ on the emission spectrum of PBFI. Panel A shows the emission spectra of PBFI as a function of increasing KCl. Panel B shows the difference in emission intensity between the K^+-free and K^+-bound indicator. Conditions: 1 μM PBFI, 10 mM tetrabutylammonium phosphate, 1 mM EDTA, pH 7.0, 25 °C. [KCl] ranged from 0.0035 to 138 mM. Fluorescence intensity is given in count/s.

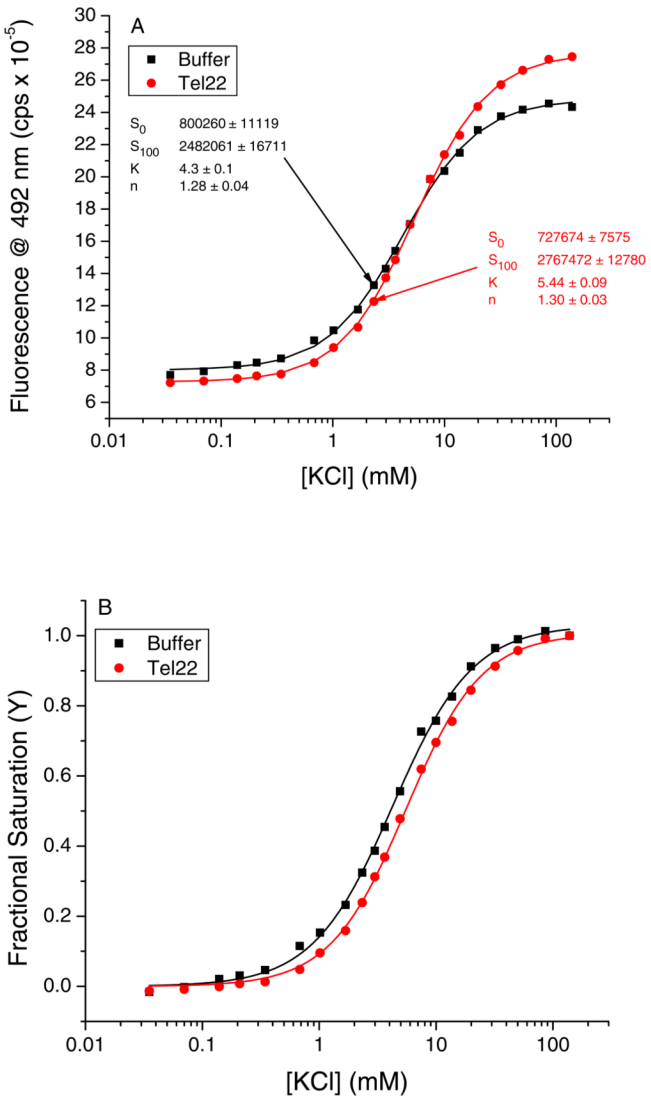

Fig. 6.

K^+-PBFI titration curves in the absence and presence of Tel22. Panel A shows the fluorescence intensity at 492 in counts/s. The lines represent the best fit of the points to Eq. 1. The fitted parameters and their standard deviations are shown in the figure. Panel B shows the data of panel A normalized using Eq. 2 and the optimized values of S_0 and S_{100}. [Tel22] = 458 μM in panel B; other conditions were the same as in Fig. 5.

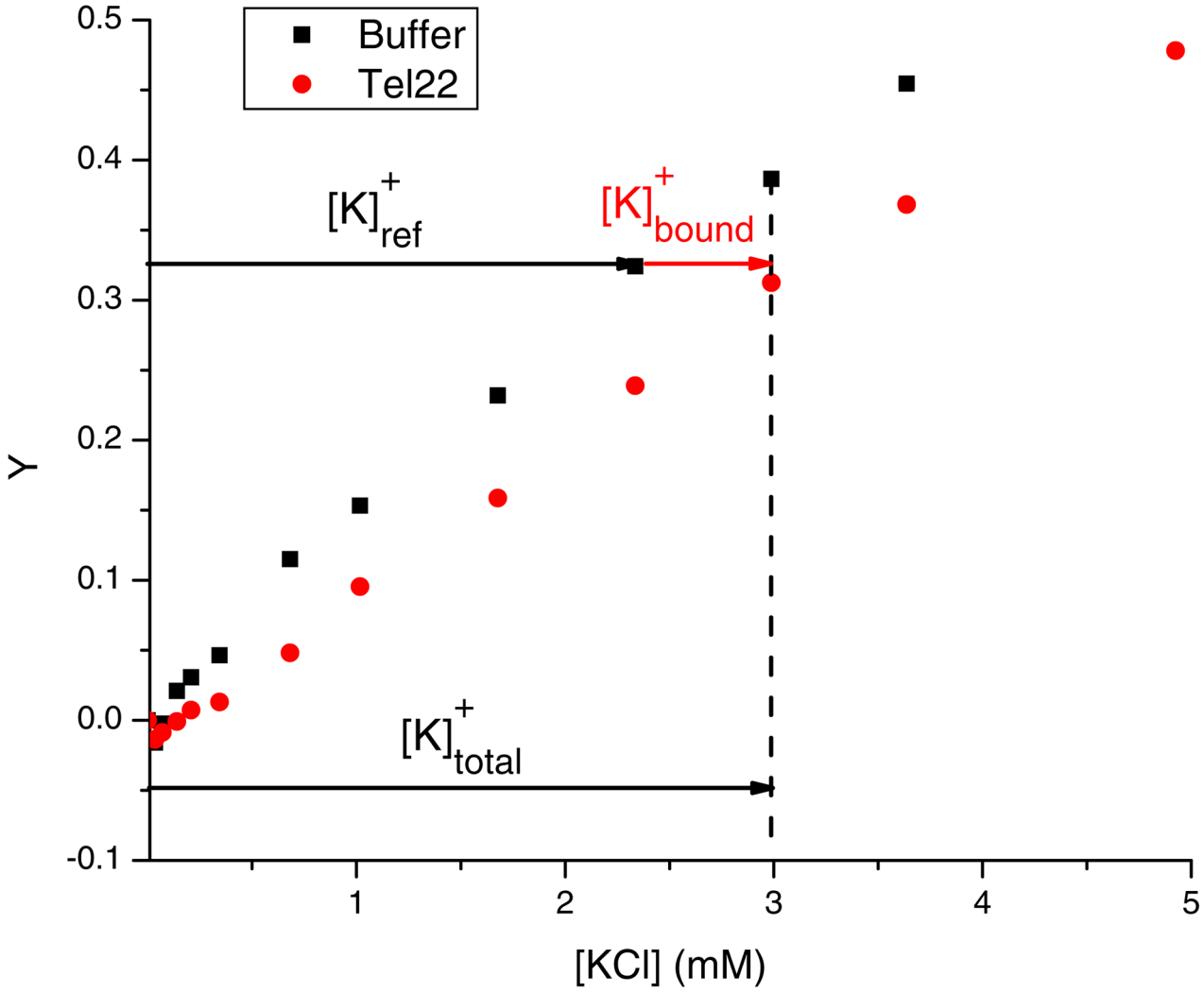

Fig. 7.
Detailed analysis of a fluorescence titration of PBFI with KCl in Fig. 5 illustrating estimation of bound and free K^+ from the relationship $[K^+]_{bound} = [K^+]_{total} - [K^+]_{ref}$.

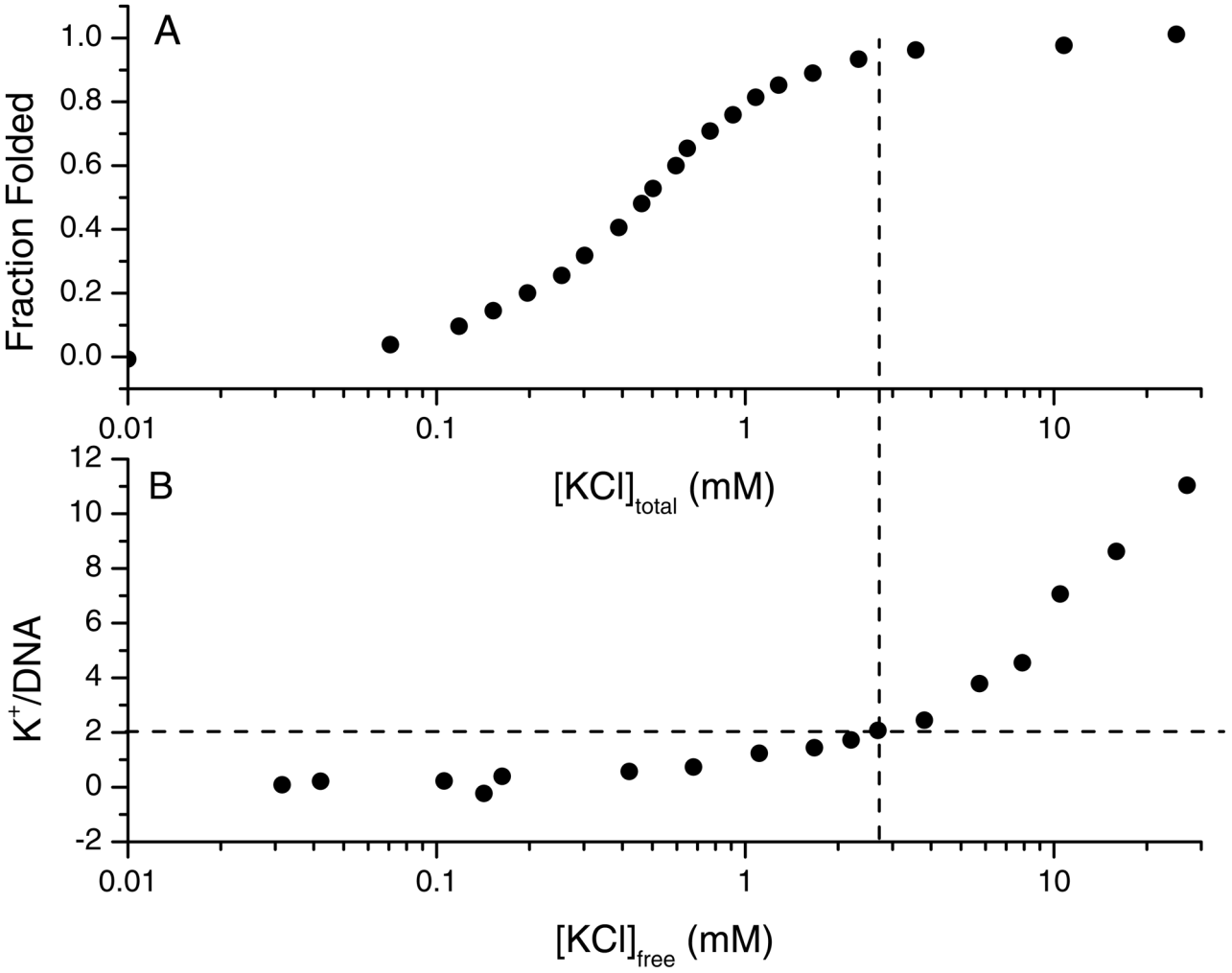

Fig. 8.
Comparison of the extent quadruplex formation as determined by CD with K^+ binding stoichiometry as determined by K^+-PBFI indicator titrations. Note that ~95% folding as determined by CD corresponds to 2 K^+/DNA. The PBFI data are from [31].

$K^+ + PBFI \bullet K^+\text{-}PBFI$	$K_{PBFI} = 5.1$ mM
$K^+ + DNA \bullet K^+\text{-}DNA$	$K_{DNA1} = 1.0$ mM
$K^+ + K^+\text{-}DNA \bullet K^+_2\text{-}DNA$	$K_{DNA2} = 0.001$ mM

Scheme 1.

Table 1

Summary of singular values and relative variances of the five most significant components of the titrations in Figure 2 derived by singular value decomposition.

	CD Data		Absorbance Data	
Component	**Singular Value**	**Relative Variance (%)**	**Singular Value**	**Relative Variance (%)**
1	550.89	95.61	2.08	95.81
2	116.74	4.29	0.43	4.16
3	10.97	0.04	0.03	0.02
4	7.30	0.02	0.02	0.01
5	5.83	0.01	0.01	0.00